atmosphere

MDPI

Article

Identification of a Function to Fit the Flow Duration Curve and Parameterization of a Semi-Arid Region in North China

Lan Ma [1], Dengfeng Liu [1,*], Qiang Huang [1], Fengnian Guo [1], Xudong Zheng [1], Jing Zhao [1], Jinkai Luan [2], Jingjing Fan [1,3] and Guanghui Ming [4]

[1] State Key Laboratory of Eco-Hydraulics in Northwest Arid Region of China, School of Water Resources and Hydropower, Xi'an University of Technology, Xi'an 710048, China
[2] Key Laboratory of Water Cycle and Related Land Surface Processes, Institute of Geographic Sciences and Natural Resources Research, Chinese Academy of Sciences, Beijing 100101, China
[3] School of Water Conservancy and Hydroelectric Power, Hebei University of Engineering, Handan 056002, China
[4] Key Laboratory of Water Management and Water Security for Yellow River Basin (Ministry of Water Resources), Yellow River Engineering Consulting Co., Ltd., Zhengzhou 450003, China
* Correspondence: liudf@xaut.edu.cn

Abstract: The discharge process has undergone major changes in many river basins throughout the world as a result of the simultaneous influences of global climate change and human activity. Flow duration curves (FDCs) are crucial indicators of river basins' hydrological processes. However, it is challenging to compare FDCs in a quantitative way. This study will identify the best function with which to fit the flow duration curve in a semi-arid region of North China, so as to quantify the FDC, and parameterize the function of the FDC of the region in order to describe the FDCs of ungauged basins. In this work, six small- and medium-sized catchments in North China are selected as the study area, and three functions, i.e., log normal, generalized Pareto and H2018 functions, were chosen to fit the FDC at nineteen hydrological stations. The relationship between the parameters of the FDC and the basin characteristics, such as the climatic factors and geographical features, were analyzed. A regression formula of the parameters of the FDC function was established, and its spatial and temporal distributions were examined. Based on the evaluation of four indicators, the Nash–Sutcliffe efficiency, the root mean square relative error, the logarithmic Nash efficiency coefficient and the coefficient of determination, the results demonstrate that the H2018 function can match FDCs the best. Through the annual runoff, annual precipitation, precipitation in summer, potential evapotranspiration, catchment area, mean elevation, length of the main channel and maximum flow frequency, the parameters of a, b, and k in the H2018 function can be formulated. The regression formula constructed in this study can obtain a regional flow duration curve with satisfactory performance, which provides a reference for the validation of remote-sensing-based runoff data in ungauged regions.

Keywords: flow duration curve; parameterization; runoff; variation

Citation: Ma, L.; Liu, D.; Huang, Q.; Guo, F.; Zheng, X.; Zhao, J.; Luan, J.; Fan, J.; Ming, G. Identification of a Function to Fit the Flow Duration Curve and Parameterization of a Semi-Arid Region in North China. *Atmosphere* **2023**, *14*, 116. https://doi.org/10.3390/atmos14010116

Academic Editors: Tianye Wang, Hongshi Xu, Ping Wang and Shiqin Xu

Received: 15 December 2022
Revised: 2 January 2023
Accepted: 3 January 2023
Published: 5 January 2023

1. Introduction

It is still a major challenge to scientifically and efficiently manage the water resources in basins, which is primarily due to a lack of hydrological data. The International Association of Hydrological Sciences (IAHS) put forward hydrological projections for basins without data, which are predictions in ungauged basins (PUBs) [1]. This is one of the key and difficult problems in hydrology research and has received extensive attention from many scholars [2–5]. In basins with no data or a lack of data, it is difficult to establish a plan for regional water resources.

However, there are only a certain number of gauging stations worldwide, and this number is decreasing as a result of funding reductions (i.e., not all streams are gauged). Generally, there are two methods for runoff process research in ungauged basin [6]: One is

to establish a watershed hydrological model that only contains physical parameters. Since the model parameters may be measured, they can be used directly in the areas without data. The alternative option is to build a watershed hydrological model with parameters that will be calibrated, in which the model parameters of regions with data are simulated and applied to regions without data [7,8].

FDCs can capture the properties of precipitation and runoff by building a statistical relationship between them, and they have been widely applied in various fields of hydrology [9–12]. FDCs are built in two main steps: ranking the streamflow data in descending order and plotting the sorted values against the corresponding frequency of exceedance [13]. As a graphical representation of the relationship between flow frequency and flow rate can be simple and comprehensive, an altered graphic with which to describe the whole study period of runoff, from low water to flood characteristics of the traffic condition, can better reflect the basin rainfall runoff characteristics, and it also can be applied into water resources exploitation and protection.

A method with which to estimate the FDCs of ungauged sites based on distance measures that can be related to the catchment area and the climatic parameters has been established by many authors that addressed the topic of FDC prediction at ungauged or partially gauged locations through regional regression [14–17] and geostatistical interpolation [18]. Spatial nonlinear interpolation methods were developed by several scholars [19–21]. Worland et al. (2019) [22] presented a method involving the use of the copula function. Hughes and Smakhtin (1996) [23] proposed a method with which to extend or fill in daily flow time series at a site by using the monthly FDCs of a target site itself.

The Loess Plateau is located in the middle and upper reaches of the Yellow River, with fragile ecological environment and soil erosion [6,24]. With global climate change, the frequency of extreme climate events increases, and the risk of meteorological disasters intensifies. Furthermore, the rivers of the Loess Plateau are under the dual effects of global climate change and human activities; significant changes in flow processes have occurred, and the smallest watersheds are ungauged basins without observational flow data [25]. The National Development and Reform Commission of the Ministry of Water Resources officially issued and implemented the 14th five-year implementation plan for the construction of warping dams in the Yellow River basin and the comprehensive control of soil and water loss in sloping farmland [26], which intends to, over a period of five years, build 1461 warping dams and 2559 sand-blocking dams in the concentrated source area of coarse sediment. A large number of silt dams for soil and water conservation are constructed in small watersheds with no discharge data. If the FDCs of small watersheds can be constructed by regionalization of parameters, they will provide an important reference for the construction of warping dams in small watersheds.

The primary method used in the current study on FDCs is the construction of a trustworthy fitting function with which to infer the flow processes in an ungauged basin. The shapes of FDCs have strong regional differences. Preliminary studies on the Loess Plateau have shown that the low-flow part of the flow duration curve of the Yellow River basin will rapidly decrease and show an obvious S-shape. Blum et al. (2017) [27] omitted intermittent sites with an average daily flow value of zero from their analysis because such intermittent sites require additional methodological considerations. Therefore, it is necessary to optimize the function form of the optimal FDC on the Loess Plateau and to construct a calculation formula of the parameters. Based on this, this study proposed constructing an FDC, analyzing the influential elements of the curve shape, and studying the variation in the parameters of the FDC on both the temporal and spatial scales. Due to the influence of both global climate change and human activities, important signatures of the hydrological processes of river basins have changed significantly, especially flow duration curves (FDCs). However, FDCs are difficult to quantitatively compare and differ between different basins due to climatic and basin characteristics. The shapes of the curves vary greatly between basins. For instance, the research finds that FDCs display an 'L-shape' in the Americas [28]; however, the distribution runoff process in North China exhibits

an 'S-shape'. With this being the case, the H2018 function [29] has been put forward to describe the FDC of this study area. Therefore, it is necessary to study the variation of the FDC of this basin and obtain FDCs in ungauged regions via parametric analyses without discharge data. Additionally, the parametric formula of the FDC can be applied to validate the remote-sensing-based runoff data in ungauged basins.

The study is organized as follows. Section 2 presents the study area and data. Section 3 presents the methodology employed to fit FDCs at hydrological stations. Section 4 presents the main results. Section 5 discusses the results in a catchment. Section 6 concludes the study and highlights the outlook for further research based on our finding.

2. Study Area and Data

2.1. Study Area

In this study, six small- and medium-sized watersheds of the Loess Plateau in North China were selected as the study watersheds, covering 58,677.54 km^2, as shown in Figure 1. They include the Wuding River basin, Jialu River basin, Tuwei River basin, Kuye River basin, Gushan River basin, and Huangfu River basin.

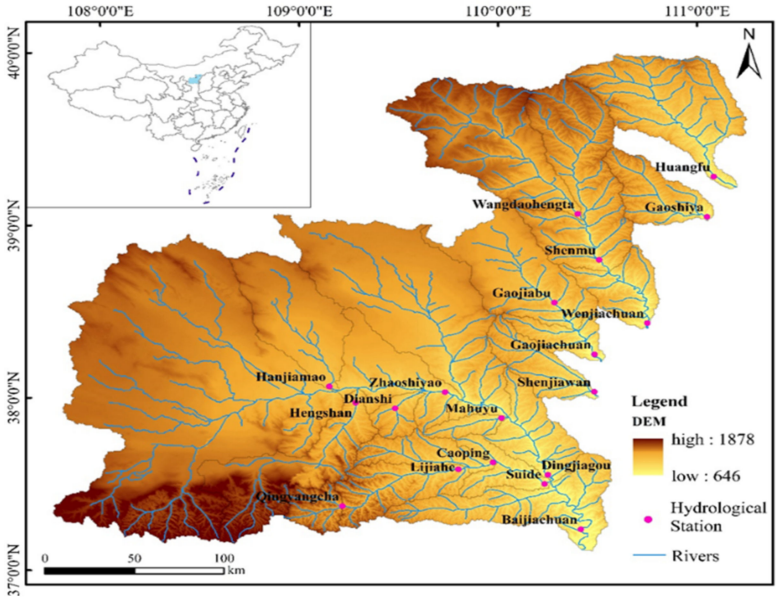

Figure 1. The distribution of the six watersheds and nineteen hydrological stations.

The landform types of the northern Shaanxi region are mainly the aeolian sand transition area and the Loess Plateau area with sparse vegetation, and the region is one of the areas of China with serious levels of soil erosion and desertification [30,31]. It has a typical warm temperate continental monsoon climate, with a cold and dry winter, and a warm and rainy summer. The average annual temperature is 3.6~14.3 °C, and the annual rainfall is 300~800 mm; 65% of the precipitation occurs mainly in the summer (June to September) [32].

2.2. Data

In this study, the daily runoff data of the 19 hydrological stations in the six watersheds, as shown in Figure 1, were obtained from the hydrological data of the Yellow River. Due to the lengths of the observed data being inconsistent, the longest data sequence is from 1955 to 2012, and the shortest is from 1975 to 2012. The length of the data series is sufficient for this research. Furthermore, in order to explore the factors influencing FDCs, regional meteorological characteristics and watershed characteristics data were extracted, as shown in Table 1, including the sub-basin area covered by hydrological stations, A (km^2), the average annual precipitation, P (mm), the average annual precipitation in summer, P_{summer}

(mm), the average annual potential evapotranspiration in the sub-basins, E_p (mm), the annual runoff, R (10^8 m^3), the mean elevation of the sub-basins, H (m), the length of the main channel, L, and the elevation difference of the sub-basins, ΔH (m) [33].

Table 1. Geomorphological and climatic factors for the catchments of hydrological stations.

Hydrological Station	A (km^2)	P (mm)	P_{summer} (mm)	E_p (mm)	R (10^8 m^3)	L (km)	ΔH (m)	H (m)
Huangfu	3279.66	405.03	69.66	1028.39	1.2639	115.0803	628	1159.31
Qingyangcha	673.27	495.09	90.80	1041.21	0.2769	26.2307	530	1378.66
Shenjiawan	1147.43	444.33	77.14	1042.19	0.6067	63.0707	639	1125.8
Suide	3902.10	471.71	85.08	1136.6	1.4241	140.2538	901	1202.32
Dianshi	467.09	435.27	78.25	1143.29	0.1923	32.6463	383	1172.77
Hanjiamao	2574.20	349.51	63.02	1195.34	0.8387	109.4724	428	1271.81
Dingjiagou	30,123.08	347.69	67.69	1168.87	8.6968	312.9130	1058	1291.17
Gaojiachuan	3505.83	427.83	73.34	1117.67	3.3177	122.4448	638	1171.09
Lijiahe	821.04	441.04	79.02	1150.79	0.3394	50.4180	473	1183.01
Mahuyu	376.91	449.85	80.01	1124.49	0.6232	32.6446	399	1098.68
Gaojiabu	2138.81	417.75	71.32	1147.51	2.5568	68.5825	408	1223.6
Gaoshiya	1274.63	426.27	72.72	961.29	0.4734	65.1414	580	1176.28
Hengshan	2750.67	433.15	79.75	1084.73	0.6441	130.1403	799	1385.72
Baijiachuan	36,485.42	371.12	71.00	1167.53	9.4079	371.9764	1206	1265.55
Caoping	205.52	450.14	80.05	1186.35	0.0682	17.5944	308	1075.25
Zhaoshiyao	22,138.10	368.02	67.88	1185.08	4.5628	234.6551	946	1329.69
Shenmu	6930.95	390.07	65.30	1338.47	4.5651	139.3944	628	1300.3
Wenjiachuan	12,517.48	278.69	46.88	1293.97	5.1815	206.0730	818	1260.1
Wangdaohengta	3833.95	378.28	62.94	1431.29	1.8385	119.4600	557	1332.49

The DEM data used in this study were from the official website of the US Geological Survey, and which were extracted from the NASA Advanced Spaceborne Thermal Emission and Reflection Radiometer Global Digital Elevation Model (ASTER GDEM) with a spatial resolution of 30 m. The precipitation data (1961–2015) were from China's ground precipitation monthly value 0.5 × 0.5 grid data set (V2.0), from the China Meteorological Data Sharing Service Network (http://data.cma.cn) on 1 October 2022.

3. Methods

Three functions, i.e., log normal function, generalized Pareto function and H2018 function, were selected to simulate FDC through four assessment indices, i.e., the Nash–Sutcliffe efficiency, the root mean square relative error, the logarithmic Nash efficiency coefficient, and the coefficient of determination. Additionally, a regression model was then used to construct the formulae of the parameters.

3.1. Log Normal Function

If the function Y = lnX of the random variable x obeys the normal distribution $N(\mu, \sigma^2)$, the probability density function of the lognormal distribution of x obeys the parameters μ and σ^2 is said to be as follows:

$$f(x) = \frac{1}{x\sqrt{2\pi}\sigma} \exp[-\frac{1}{2\sigma^2}(\ln x - \mu)^2] \quad (1)$$

where X is the random variable, and x is the independent variable of the probability density function, μ is the logarithmic mean parameter, and σ is the logarithmic variance parameter, as well as the scale parameter.

3.2. Generalized Pareto Function

If X obeys the generalized Pareto function $GPD(\mu,\ \sigma,\ \xi)$, then its cumulative distribution function is as follows:

$$F_{(\mu,\sigma,\xi)}(X) = 1 - (1 + \frac{\xi(X-\mu)}{\sigma})^{-1/\xi} \tag{2}$$

where $\xi \neq 0$.

Its corresponding distribution density function (PDF) is as follows:

$$f_{(\mu,\sigma,\xi)}(x) = \frac{1}{\sigma}(1 + \frac{\xi(x-\mu)}{\sigma})^{(-\frac{1}{\xi}-1)} \tag{3}$$

3.3. H2018 Function

Han and Tian [29] proposed a new function of the form below:

$$y = \frac{1}{1 + m\left(\frac{x_{max}-x}{x-x_{min}}\right)^n} \tag{4}$$

where m and n are the parameters, $x_{min} \leq x \leq x_{max}$.

In flow duration curve fitting, when the frequency increases from 0 to 1, the flow gradually decreases, and the function in the original form needs to be transformed, such that the modified H2018 function form is as follows:

$$y = \frac{a}{1 + b\left(\frac{x}{x_{max}-x}\right)^k} \tag{5}$$

3.4. Evaluation Indices

In this study, the Nash–Sutcliffe efficiency (*NSE*) [17,34,35], the root mean square relative error (*RMSRE*) [36], the logarithmic Nash–Sutcliffe efficiency coefficient (*LNSE*) and the coefficient of determination (R^2) [37–39] were used to evaluate the applicability of different distribution functions at the hydrological station.

The Nash efficiency coefficient (*NSE*) is an evaluation parameter used to evaluate model quality and is generally used to verify the quality of hydrological model simulation results. The *NSE* is defined as follows:

$$NSE = 1 - \frac{\sum_{t=1}^{T}(Q_o^t - Q_m^t)^2}{\sum_{t=1}^{T}(Q_o^t - \overline{Q}_o)^2} \tag{6}$$

where Q_o^t refers to the observed value, Q_m^t refers to the simulated value, Q^t represents a certain value at time t, and $\overline{Q}_o$ represents the total average of the observed value.

The value of the *NSE* is from negative infinity to 1, and if the *NSE* is close to 1, this indicates good model quality and high model reliability. If the *NSE* is close to 0, this indicates that the simulation result is close to the average level of the observation value, that is, the overall result is reliable, but the process simulation error is large. If the *NSE* is much less than 0, the model is not credible.

The logarithmic Nash efficiency coefficient (*LNSE*) is an evaluation parameter calculated by taking the logarithms of observed and simulated values. The specific calculation formula is as follows:

$$LNSE = 1 - \frac{\sum_{t=1}^{T}(\ln Q_o^t - \ln Q_m^t)^2}{\sum_{t=1}^{T}(\ln Q_o^t - \ln \overline{Q}_o)^2} \tag{7}$$

In the formula, $\ln Q_o^t$ refers to the logarithm of the observed value, $\ln Q_m^t$ refers to the logarithm of the simulated value, and $\ln \overline{Q}_o$ refers to the logarithm result of the total average of the observed value.

The root mean square relative error, also known as the standard error, is the square root of the ratio between the sum of squares of the deviation between the observed value and the truth value and the number of observations, m, which measures the deviation between the observed value and the truth value. *RMSRE* is calculated as follows:

$$RMSRE = \sqrt{\frac{1}{N}\sum_{t=1}^{N}\left(\frac{Q_o^t - Q_m^t}{Q_o^t}\right)^2} \quad (8)$$

where N is the number of samples, Q_o^t is the observed value and Q_m^t is the simulated value.

The coefficient of determination (R^2) is the square of the Pearson correlation coefficient and is a kind of non-deterministic relation, and is a quantity used to study the degree of linear correlation between variables.

3.5. Multiple Regression

Regressive methods have been used to link the different model parameters to some catchment characteristics such as climatic indices, land coverage, and geological and geomorphological parameters. This analysis was performed in this study by dividing the island into 19 subzones. The regressive formula used in this study has the following structure [40]:

$$y = k_0 + \sum_{i=1}^{n} k_i C_i \quad (9)$$

where y represents the parameters used in the function which has been chosen, parameters k_0 and k_i are determined through a regression analysis.

Multiple regression examines how multiple independent variables are related to one dependent variable. Once each of the independent factors has been determined to predict the dependent variable, the information on the multiple variables can be used to create an accurate prediction on the level of effect that they have on the outcome variable.

3.6. Mann–Kendall Test

The Mann–Kendall test, one of the non-parametric statistical test procedures, is frequently utilized by domestic and international researchers due to its simplicity and effective application; it is particularly useful for the investigation of hydrology, meteorology, and other non-normal distribution data. In this study, the absolute value of U is larger than 1.645, which means that it has passed the significant two-sided test of 0.1 when the Mann–Kendall test is applied for the trend test, and the reliability is 0.1 [41,42].

4. Results

4.1. Best Fitting of the FDC

All of the observed flows at the 19 hydrological stations were used to fit the function for the FDC. Additionally, the best function was chosen from the log-normal distribution, generalized Pareto distribution (GPD), and H2018 distribution. Tables 2 and 3 show the values of the *LNSE*, *NSE*, *RMSRE*, and R^2 at each station, respectively.

For comparison, the LNSE had better performance than the H2018 simulation, with a maximum value of 0.9906 at the Shenmu station and a minimum value of 0.7685 at the Zhaoshiyao station. The highest values of the NSE were mostly in the H2018 simulation (the maximum value reached was 0.9515 at the Baijiachuan station). The RMSRE was lower in the simulation of H2018 and the GPD function compared to the log-normal function, and the lowest value occurred at the Wangdaohengta station. Additionally, the correlation coefficient performed well in both the H2018 and log-normal functions; the best one was 0.9800 at the Baijiachuan station. It is thus proven that the H2018 function was most effective

in terms of the best fitting of the FDC through comprehensive judgment. Furthermore, Table 4 shows the best-fitted parameters of the H2018 function.

Table 2. The values of the *LNSE* and *NSE*.

Station	*LNSE*			*NSE*		
	Log Normal	**GPD**	**H2018**	**Log Normal**	**GPD**	**H2018**
Huangfu	−0.1354	0.4516	0.9657	-6.0465×10^{31}	0.1940	0.7390
Qingyangcha	0.0253	0.1354	0.8442	-9.7243×10^{13}	−5433.4000	0.5098
Shenjiawan	0.4110	0.5623	0.9496	-5.1788×10^{10}	−0.0047	0.6080
Shenmu	0.3101	0.9630	0.9906	-9.2092×10^{16}	0.5304	0.6072
Wenjiachuan	0.3325	0.7158	0.9693	-6.9900×10^{12}	−0.0001	0.8152
Suide	0.3066	0.9180	0.7868	-4.0192×10^{6}	−4.9491	0.5575
Wangdaohengta	0.4216	0.9003	0.9700	-3.7119×10^{12}	−0.0334	0.6194
Dianshi	0.6238	0.5122	0.9517	-1.5541×10^{3}	−0.0001	0.0091
Hanjiamao	−4.5891	0.8020	0.7833	-1.1153×10^{18}	0.0672	0.4122
Dingjiagou	0.1558	0.8162	0.9075	−80.4591	0.0401	0.4045
Gaojiachuan	−14.7743	0.1337	0.9449	-8.2734×10^{35}	0.0009	0.0904
Lijiahe	0.2703	0.7719	0.9588	-2.6045×10^{6}	0.0000	0.1052
Mahuyu	0.4604	0.6021	0.9482	-6.0553×10^{6}	−0.0001	0.0060
Gaojiabu	0.2834	−1.2087	0.9711	-1.3548×10^{3}	0.0033	0.0311
Gaoshiya	−3.6981	0.7777	0.9193	-4.2702×10^{75}	0.6476	0.7357
Hengshan	−0.0318	0.7106	0.9852	-1.9970×10^{9}	0.0120	0.3849
Baijiachuan	0.2136	0.8457	0.9004	-5.5778×10^{6}	0.1465	0.9515
Caoping	0.5030	0.5682	0.9647	-2.5749×10^{8}	−0.0048	0.5006
Zhaoshiyao	−0.8401	0.8173	0.7685	6.0750×10^{22}	0.0146	0.1287

Table 3. The values of the *RMSRE* and R^2.

Station	*RMSRE*			R^2		
	Log Normal	**GPD**	**H2018**	**Log Normal**	**GPD**	**H2018**
Huangfu	1.68×10^{14}	0.0194	0.0110	0.5337	0.4569	0.9078
Qingyangcha	7.9230×10^{4}	0.5923	0.0056	0.7619	0.8896	0.7640
Shenjiawan	3.0760×10^{3}	0.0135	0.0085	0.7461	0.1048	0.9348
Shenmu	3.4500×10^{6}	0.0078	0.0071	0.6154	0.7446	0.9340
Wenjiachuan	4.6400×10^{4}	0.0175	0.0075	0.4611	0.2487	0.9493
Suide	16.3130	0.0198	0.0054	0.7524	0.9007	0.7868
Wangdaohengta	1.5051×10^{4}	0.0079	0.0048	0.7612	0.9246	0.7929
Dianshi	0.2828	0.0072	0.0071	0.7641	0.0173	0.3347
Hanjiamao	1.4565×10^{7}	0.0133	0.0106	0.7214	0.2754	0.6483
Dingjiagou	0.0854	0.0093	0.0073	0.9464	0.2197	0.6731
Gaojiachuan	6.6080×10^{15}	0.0073	0.0069	0.7855	0.0695	0.3794
Lijiahe	12.0538	0.0075	0.0071	0.8557	0.0343	0.6102
Mahuyu	19.4072	0.0079	0.0079	0.8973	0.0112	0.4910
Gaojiabu	0.2870	0.0078	0.0077	0.7243	0.0711	0.2363
Gaoshiya	8.75 × 1035	0.0080	0.0069	0.5539	-	0.8954
Hengshan	3.6975×10^{2}	0.0082	0.0065	0.8522	0.1668	0.6987
Baijiachuan	56.2953	0.0220	0.0053	0.5350	0.4491	0.9800
Caoping	2.0976×10^{2}	0.0131	0.0092	0.6467	0.1350	0.9192
Zhaoshiyao	3.0736×10^{6}	0.0072	0.0068	0.7999	0.4100	0.4076

The stations with optimal parameter values of H2018 function fitting were then selected, and a fitting effect diagram of the three functions on FDCs was drawn, as shown in Figure 2 (the Baijiachuan, Shenmu, Wenjiachuan, Huangfu, and Hengshan stations). The Huangfu station obviously indicates that the maximum frequency was lower than 0.6, which was mainly triggered by a large number of days without runoff production. Overall,

the H2018 function can fit the variation in the flow processes better, especially for the heads and tails of the observed curves.

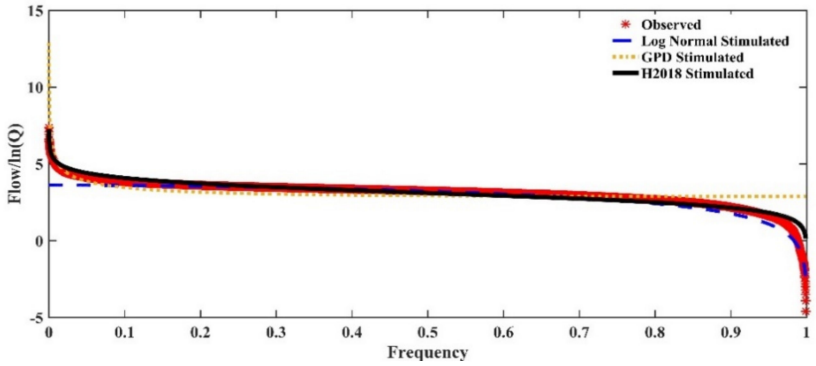

(**a**) Baijiachuan

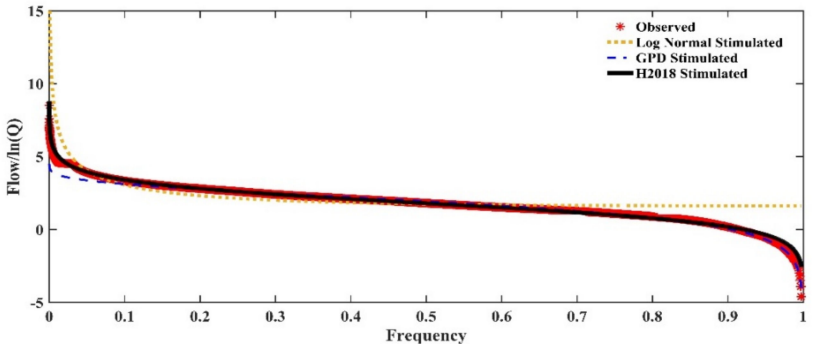

(**b**) Shenmu

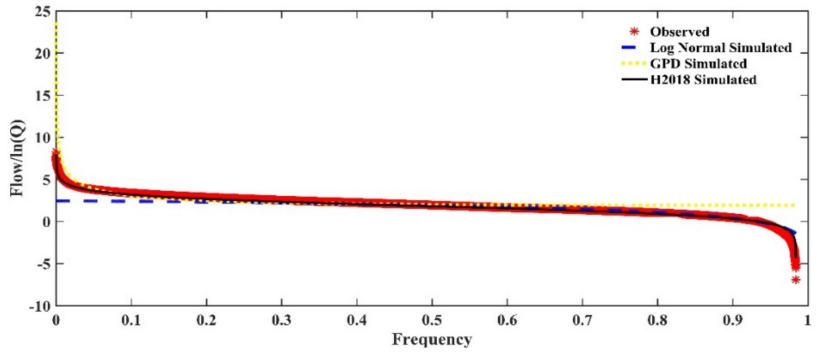

(**c**) Wenjiachuan

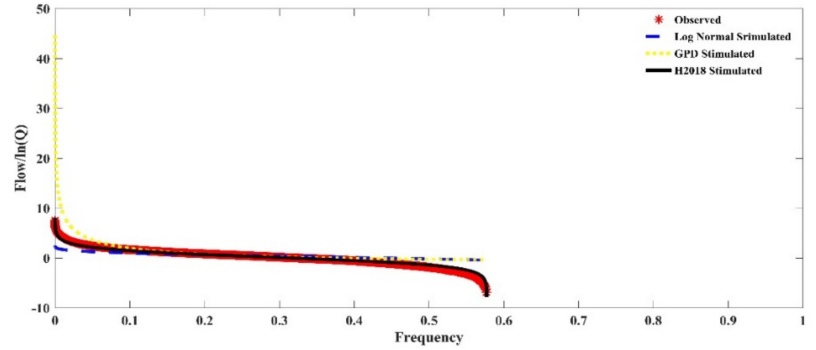

(**d**) Huangfu

Figure 2. *Cont.*

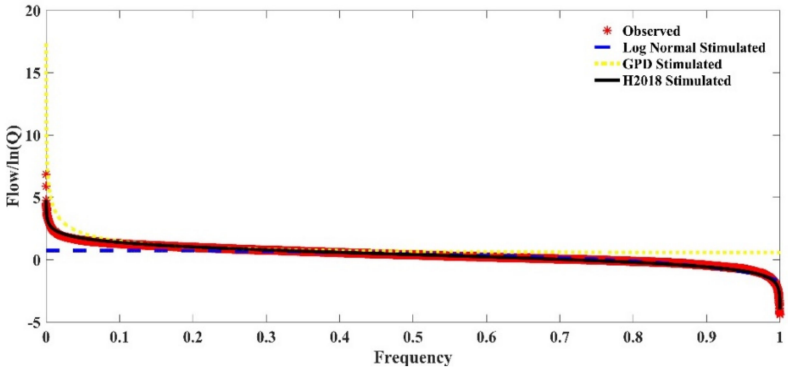

(**e**) Hengshan

Figure 2. Observed and simulated flow duration curves.

Table 4. The best-fitted parameters of the H2018 function.

Station	*a*	*b*	*k*	x_{max}
Huangfu	2.2906×10^4	$2.5500 \times 1 \times 10^4$	0.8505	0.5771
Qingyangcha	1.2597×10^4	1.9400×10^4	0.5595	1.0000
Shenjiawan	0.1295×10^4	0.1241×10^4	0.5954	0.9856
Shenmu	28.5827×10^4	4.9721×10^4	0.7021	1.0000
Wenjiachuan	26.5870×10^4	4.2650×10^4	0.6245	0.9839
Suide	2.0009×10^4	0.8104×10^4	0.6251	0.9919
Wangdaohengta	2.5995×10^4	1.2002×10^4	0.7699	0.9885
Dianshi	1.0043×10^4	3.9879×10^4	0.4199	0.9991
Hanjiamao	3.0510×10^4	1.2216×10^4	0.3199	1.0000
Dingjiagou	3.0000×10^4	0.1351×10^4	0.4454	0.9987
Gaojiachuan	2.0902×10^4	0.2300×10^4	0.3112	0.9576
Lijiahe	1.7906×10^4	3.9500×10^4	0.6045	0.9950
Mahuyu	2.0824×10^4	7.0983×10^4	0.5280	0.9645
Gaojiabu	2.9873×10^4	0.4179×10^4	0.2334	1.0000
Gaoshiya	2.7352×10^4	4.8779×10^4	0.8070	0.8287
Hengshan	2.9181×10^4	1.9514×10^4	0.4468	1.0000
Baijiachuan	3.8000×10^4	0.1691×10^4	0.4404	0.9989
Caoping	0.2003×10^4	1.9222×10^4	0.5554	0.9576
Zhaoshiyao	2.9940×10^4	0.2684×10^4	0.4499	0.9697

4.2. Characteristics of Fitted Curves with H2018

The Baijiachuan station is taken as an example, and the variation characteristics of the H2018 curves in Figure 2a are analyzed as shown in Figure 3. In Table 5, the flow of ten percentiles, Q_1, Q_5, Q_{10}, Q_{20}, Q_{50}, Q_{70}, Q_{80}, Q_{90}, Q_{95}, Q_{99} represent the flow at the percentiles of 1%, 5%, 10%, 20%, 50%,70%, 80%, 90%, 95%, and 99%, respectively. Each flow percentile represents a different section of the FDC: extreme high flows (Q_1 and Q_5) to extreme low flows (Q_{95} and Q_{99}) [43,44]. Low flows are of great importance for the functioning of many processes taking place in river ecosystems [45]. The low-flow thresholds adopted in drought studies usually vary between the 70th and 95th percentiles [46,47].

In order to better recognize the characteristics of fitting curves, the values of specific flow percentiles, and ratios of them, were calculated and are presented in Table 5. Q_1/Q_{99} represents the total change in the curve, Q_1/Q_{50} represents the degree of change in the front, and Q_1/Q_{99} represents the degree of change in the tail.

The results show that the curve has a great change in its entirety. The high-flow part and the low-flow part of the curve both show a descending trend. The FDC presents an 'S-shape'. Additionally, the results indicated that Q_1 is 178.6667 times Q_{99}. The change in the tail is larger than that in the front of the curve. In other words, low flows have greater variation. The above changes in the FDC indicate that the high flow is much higher than the low flow, and that the flow has significantly changed in one year. The extreme value of the flow varies greatly.

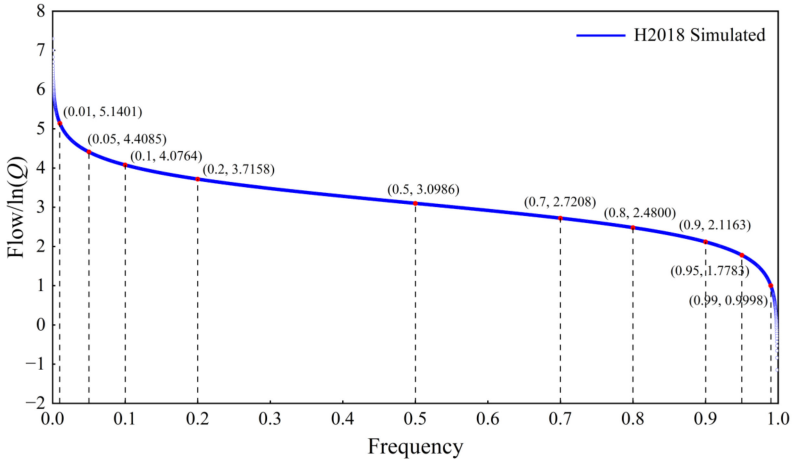

Figure 3. Flow values corresponding to different frequencies. Red circles represent the point of flow percentile.

Table 5. Values of specific flows at the percentiles at Baijiachuan.

Variables of the Percentiles	Values
$\ln Q_1$	5.1401
$\ln Q_5$	4.4085
$\ln Q_{10}$	4.0764
$\ln Q_{20}$	3.7158
$\ln Q_{50}$	3.0986
$\ln Q_{70}$	2.7208
$\ln Q_{80}$	2.4800
$\ln Q_{90}$	2.1163
$\ln Q_{95}$	1.7783
$\ln Q_{99}$	0.9998
Q_1/Q_{50}	5.2344
Q_1/Q_{99}	178.6667
Q_{50}/Q_{99}	34.1333

4.3. Formulization of Parameters

To investigate the variation in the parameters of the FDC, geomorphological and climatic factors of basins were taken into account. If the FDC can be signified by different climatic and basin characteristics, an inverse calculation will directly obtain the formula of the FDC through related factors. The main influence factors are the average annual P (mm), P_{summer} (mm), R (10^8 m^3), E_p (mm), A (km^2), ΔH (m), H (m), L (km), and x_{max}. While coal mining has a great influence on the Kuye River, this study deleted the stations (Shenmu, Wangdaohengta, and Wenjiachuan) of this basin [48]) in order to obtain better function forms of the parameters. The results indicate that the parameters of the FDC have strong relationships with A, H, L, E_p, R, P_{summer}, and x_{max}. The specific expressions calculated by multiple linear regression are as follows:

$$a = 1.1542 \times 10^{-4}R - 181.0585L - 716.4113P - 3.111 \times 10^{-14}R^2 + 0.0025 \times 10^{-4}A^2 + 0.7573P^2 + 5.1899L^2 + 0.0347PA - 0.0069PL - 0.3278AL \quad (10)$$

where the R^2 = 0.9624, $RMSRE$ = 0.0236, and P = 0.0058 < 0.01.

$$b = -45.9423A - 0.0173R - 612.7860H + 0.0021A^2 - 0.0337R^2 + 4.0180H^2 - 2.3569 \times 10^{-7}AR - 2.1412 \times 10^{-4}AL - 0.8274AH + 2.3568 \times 10^{-4}RL + 1.3409 \times 10^{-5}RH \quad (11)$$

where the R^2 = 0.9924, $RMSRE$ = 0.0224, and P = 0.0044 < 0.01.

$$k = 26.981x_{max} - 2.098P_{summer} + 0.339P - 25.05x_{max}^2 - 0.008P_{summer}^2 - 0.00014P^2 + 2.413x_{max}P_{summer} - 0.388x_{max}P + 0.002P_{summer}P - 3.604 \quad (12)$$

where the R^2 = 0.9305, *RMSRE* = 0.0494, and P = 0.0075 < 0.01.

The values of a, b, and k were calculated through the formulae constructed above (Table 6). Compared with the fitted parameter values, the simulated results are relatively similar (Figure 4). In the scatter diagrams, fitted values and simulated values all have a strong linear relationship, where the R^2 values all exceed 0.9 and the *RMSE* values are all under 0.05 (Table 7). In other words, the simulations have better results.

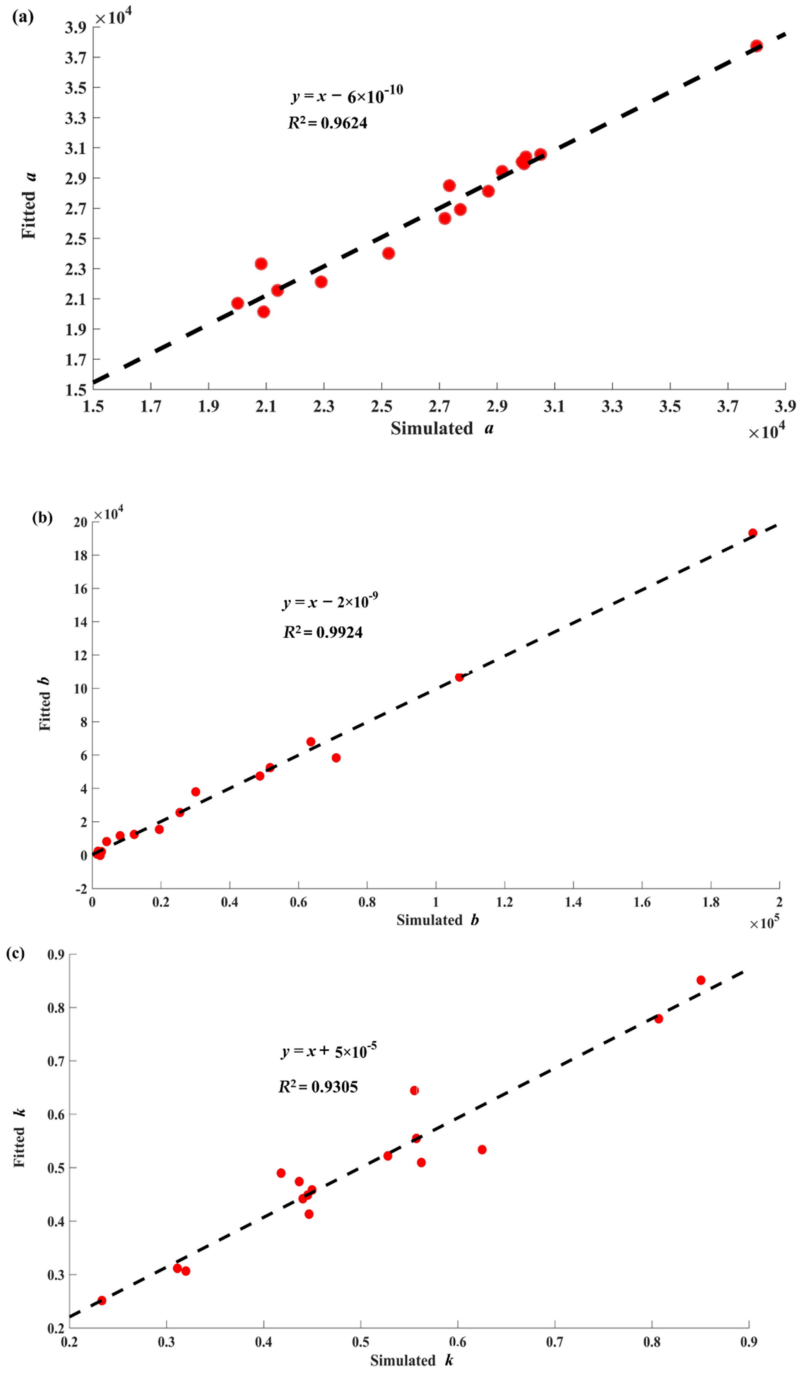

Figure 4. Scatter diagrams comparing fitted values and simulated values of (**a**) Parameter a, (**b**) Parameter b and (**c**) Parameter k. Red circles represent the points of fitted values and simulated values and dotted lines represent linear fitting.

Table 6. Comparison of calculation values.

Station	Fitted *a*	Simulated *a*	Fitted *b*	Simulated *b*	Fitted *k*	Simulated *k*
Huangfu	2.2114×10^4	2.2906×10^4	2.5500×10^4	2.5500×10^4	0.8511	0.8505
Qingyangcha	2.6906×10^4	2.7727×10^4	5.2430×10^4	5.1764×10^4	0.4738	0.4367
Shenjiawan	2.8116×10^4	2.8703×10^4	3.7916×10^4	3.0109×10^4	0.5545	0.5574
Suide	2.0703×10^4	2.0009×10^4	1.1624×10^4	0.8104×10^4	0.5335	0.6251
Dianshi	2.4002×10^4	2.5243×10^4	10.6696×10^4	10.6878×10^4	0.4896	0.4180
Hanjiamao	3.0545×10^4	3.0510×10^4	1.2410×10^4	1.2216×10^4	0.3065	0.3199
Dingjiagou	3.0385×10^4	3.0000×10^4	0.1692×10^4	0.1351×10^4	0.4485	0.4454
Gaojiachuan	2.0136×10^4	2.0909×10^4	-0.1668×10^4	0.2230×10^4	0.3116	0.3112
Lijiahe	2.6322×10^4	2.7192×10^4	6.7931×10^4	6.3613×10^4	0.5094	0.5625
Mahuyu	2.3317×10^4	2.0824×10^4	5.8293×10^4	7.0983×10^4	0.5218	0.5280
Gaojiabu	3.0067×10^4	2.9873×10^4	0.8134×10^4	0.4179×10^4	0.2513	0.2334
Gaoshiya	2.8487×10^4	2.7352×10^4	4.7378×10^4	4.8779×10^4	0.7788	0.8070
Hengshan	2.9428×10^4	2.9181×10^4	1.5422×10^4	1.9514×10^4	0.4129	0.4468
Baijiachuan	3.7741×10^4	3.8000×10^4	0.2347×10^4	0.1691×10^4	0.4417	0.4404
Caoping	2.1555×10^4	2.1393×10^4	19.3197×10^4	19.2220×10^4	0.6443	0.5554
Zhaoshiyao	2.9940×10^4	2.9940×10^4	0.2082×10^4	0.2684×10^4	0.4582	0.4499

Table 7. Comparison of fitted values and simulated values.

Index	*a*	*b*	*k*
R^2	0.9624	0.9924	0.9305
RMSRE	0.0229	0.0424	0.0494

4.4. The Spatial Distribution of Parameters

Although we calculated the above parameters in this study, how they are distributed in North China has not yet been elucidated. Therefore, the temporal and spatial variations in a, b, and k are analyzed in this part.

The specific spatial variation is simulated in Figure 5. It was found that the values in most stations are concentrated within 29,000–31,000. In addition to the great influence of basins on parameter a, the distribution of a/A was also considered. The value of b had a larger proportion from 2000 to 5000. Additionally, k was higher in the north of the basin by comparison.

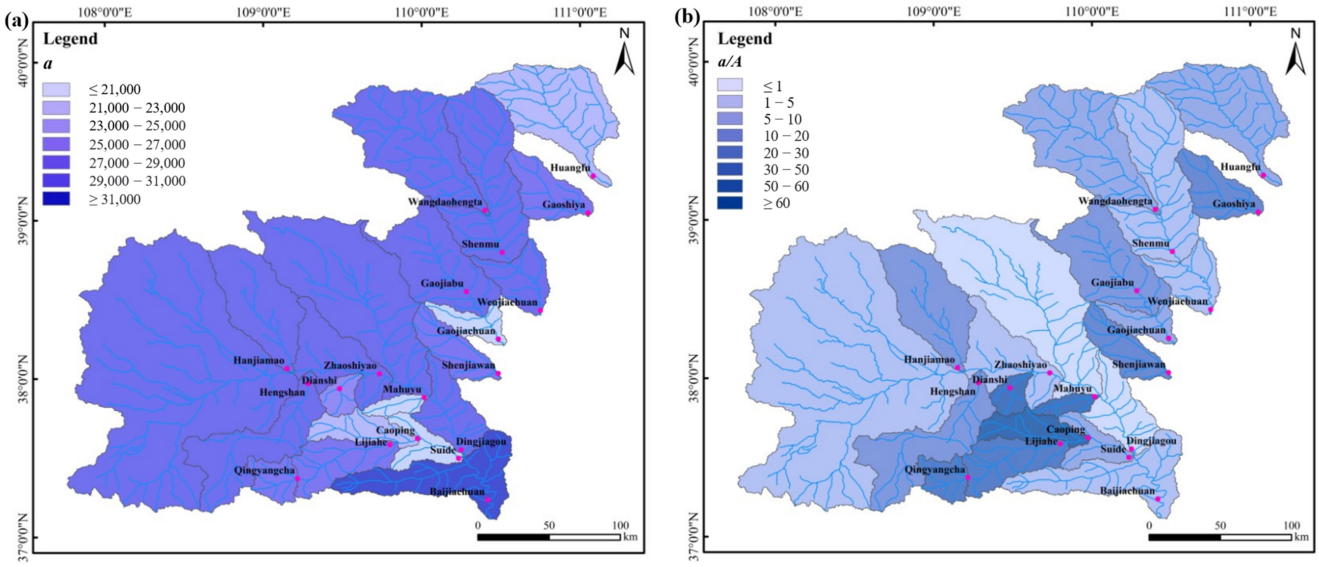

Figure 5. *Cont.*

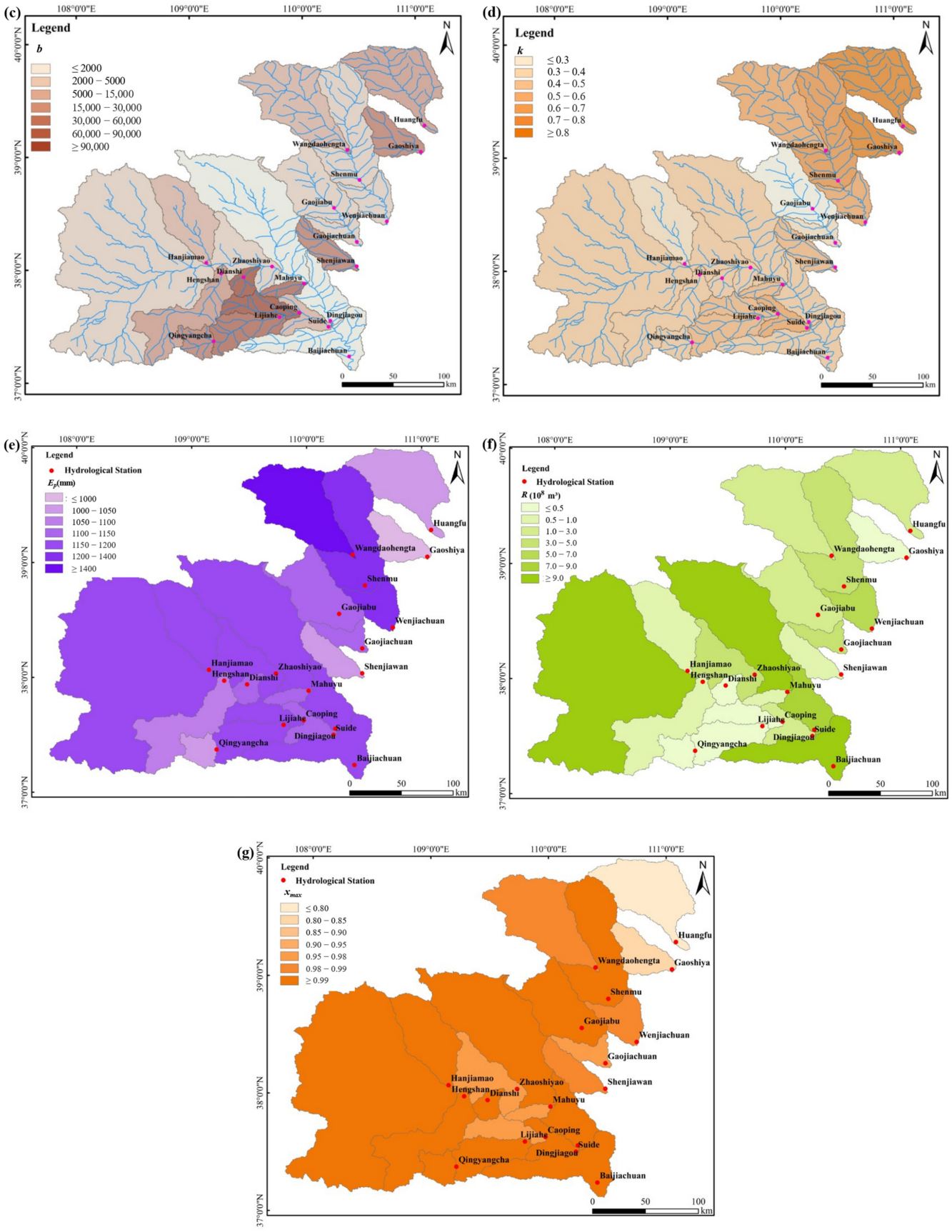

Figure 5. Spatial variation of (**a**) Parameter a, (**b**) a/A, (**c**) Parameter b, (**d**) Parameter k, (**e**) E_p, (**f**) R and (**g**) x_{max}.

In addition to the characteristics of the basin itself, E_p, R, and x_{max} had relatively large impacts on the parameters' distributions; a spatial distribution map of these three factors was drawn as Figure 5. Runoff was lower in the southeast, similar to parameter a. E_p was relatively large in the whole study area, and the majority of x_{max} exceeded 0.9.

4.5. The Temporal Distribution of Annual FDC Parameters

As for temporal variation, the Baijiachuan station (which covers the entire Wuding River basin) was chosen to study the changes in parameters a, b, and k of the FDC based on annual flow data (FDC_{ANN}) (Figure 6). The trend variation in these three parameters can be found when the test statistic Z, calculated through a Mann–Kendall test, is equal to or greater than 1.96, indicating that it exceeded the significance test with 99% confidence. The results show that a has an obvious descending trend (Z = −4.8146), b has an obvious increasing trend (Z = 4.1371), and k has an unobvious increasing trend (Z = 1.4032).

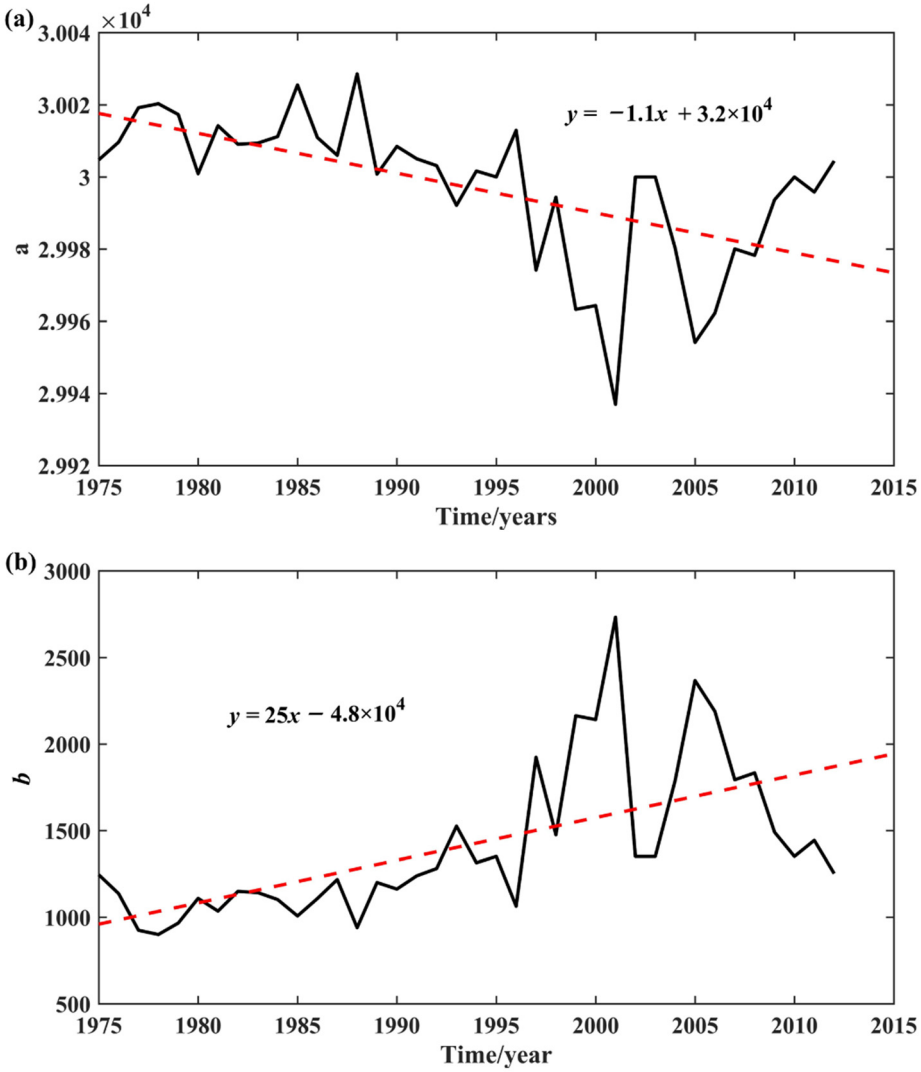

Figure 6. *Cont.*

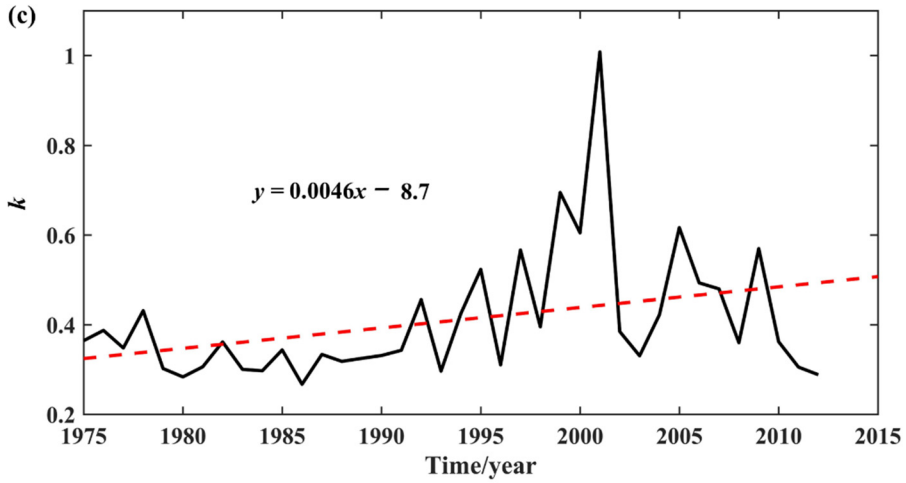

Figure 6. Temporal variation of parameters of (**a**) Parameter *a*, (**b**) Parameter *b* and (**c**) Parameter *k* at the Baijiachuan station. The solid lines represent the value of parameters and dotted lines represent the linear fitting.

According to the research findings, altering the parameter size scales and precisions of a will significantly modify the height of FDC, as shown in Figure 7. That is to say, a is mainly influenced by runoff. As can be seen from Figure 7, if only the value of a is changed, the height of the curves will shift significantly. Parameter a has changed from 8000 to 38,000 and 80,000 in Figure 7a–c, which illustrates that when *a* is higher the simulated curve will move upwards, and the Y-axis represents the volume of runoff. The result then shows that the change in a is greatly influenced by runoff. Based on this, the trend of runoff variation was analyzed. The runoff from 1975 to 2012 is similar to the variation in a, which also exhibits a declining tendency [49,50], and Z = −4.4253 via a Mann–Kendall test, which indicates a significant change.

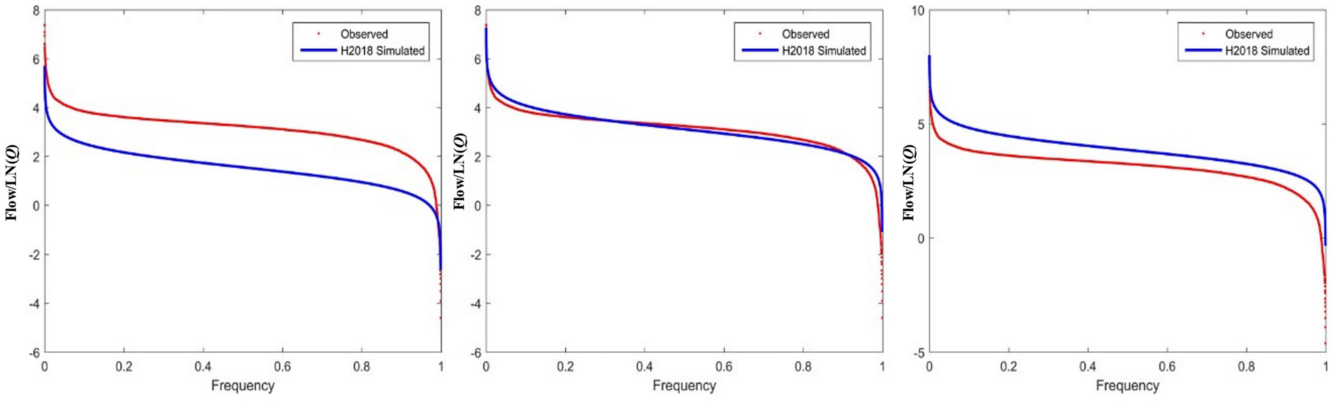

Figure 7. Change in the value of parameter a of FDC_{ANN}.

Table 8 presents the characteristic values of a, b, and k, including the average, max and min of the parameters in FDC_{ANN}. As can be seen, the min of a occurred after the year 2000, while the max of b and k appeared. Comparatively speaking, there are only tiny differences between the max and min values of a (0.3%), whereas the values of b and k change significantly (67% and 73%, respectively).

Table 8. Characteristic values of a, b, and k at the Baijiachuan station.

Parameter	Average	Max	Min
a	2.9997×10^4	3.0029×10^4	2.9937×10^4
b	0.1415×10^4	0.2732×10^4	0.0901×10^4
k	0.4089	1.0080	0.2671

5. Discussion

The FDC is investigated in this section due to the impact of coal mining and additional influences on the flow of the Kuye River. The parameters of FDC are quite different from the other river basins in this region. Figures 8–10 indicate the temporal variations in three stations (Wenjiachuan, Wangdaohengta, and Shenmu) in the Kuye River. It can be easily found that both a and b have similar tendencies, and a Mann–Kendall test shows all obvious increases or decreases. However, the variation in parameter k is inconspicuous, and it has little difference with the other two stations in Wangdaohengta. Perhaps this was caused by the inconsistent geomorphology. The Wangdaohengta station, in particular, is situated in the upstream area and belongs to the sandy area, as opposed to the other two stations, which are situated in the Loess area. In addition, the annual runoff generally exhibited a downward tendency [31], the mutational point appeared in 1996, and coal output also started to increase at that time. Additionally, the upstream rainfall erosion is the smallest erosion area.

Based on the general survey data of water conservation of the Yellow River Conservancy Committee in 2011, there were 306 key dams in the Kuye River watershed, with a total storage capacity of 316.64 Mm^3. Additionally, the majority of the dams were built in the mid-lower reaches. The regions that were at high risk of soil erosion and sediment yield were mainly concentrated in the middle reaches of the watershed [51]. The influence of human activities will affect the regional runoff variations to a large extent.

Furthermore, the characteristic values of a, b, and k at the Kuye River were also calculated (Table 9). The results indicated that the values of a are all smaller than those at the Baijiachuan station, while those of b and k are both larger. These values may affect the formulation of parameters in Section 4.3.

Table 9. Characteristic values of a, b, and k at the Kuye River.

Station	Parameter	Average	Max	Min
Wangdaohengta	a	2.9414×10^4	2.9859×10^4	2.8174×10^4
	b	1.4340×10^4	4.1827×10^4	0.4485×10^4
	k	0.5881	0.8516	0.3231
Shenmu	a	2.9785×10^4	3.0046×10^4	2.9322×10^4
	b	0.6122×10^4	1.6347×10^4	0.0321×10^4
	k	0.5962	0.9039	0.0031
Wenjiachuan	a	2.9833×10^4	2.9982×10^4	2.9480×10^4
	b	0.5049×10^4	1.2862×10^4	0.1756×10^4
	k	0.6051	0.8280	0.2301

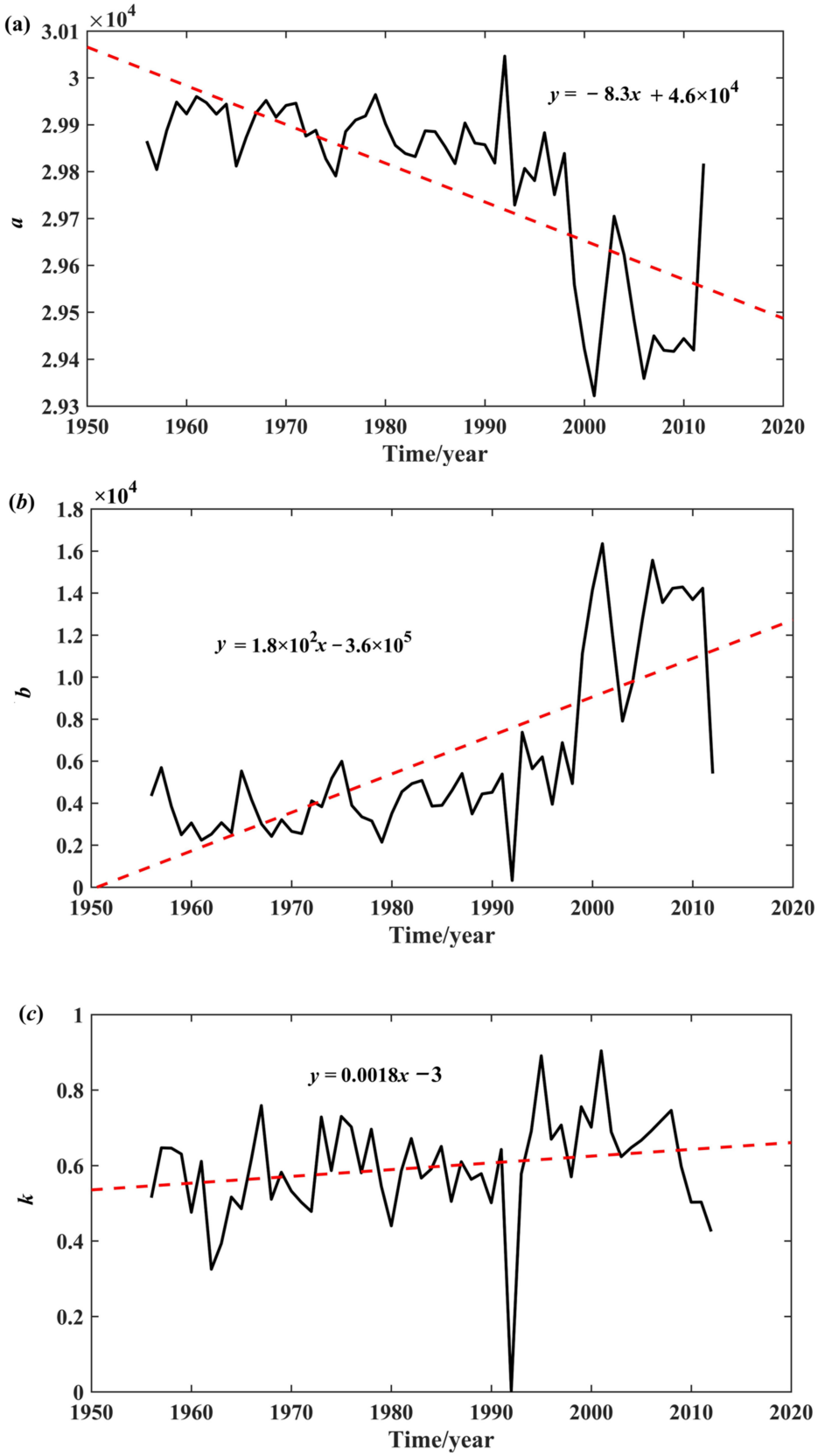

Figure 8. Temporal variation of parameters of (**a**) Parameter *a*, (**b**) Parameter *b* and (**c**) Parameter *k* at the Shenmu station. The solid lines represent the value of parameters and dotted lines represent the linear fitting.

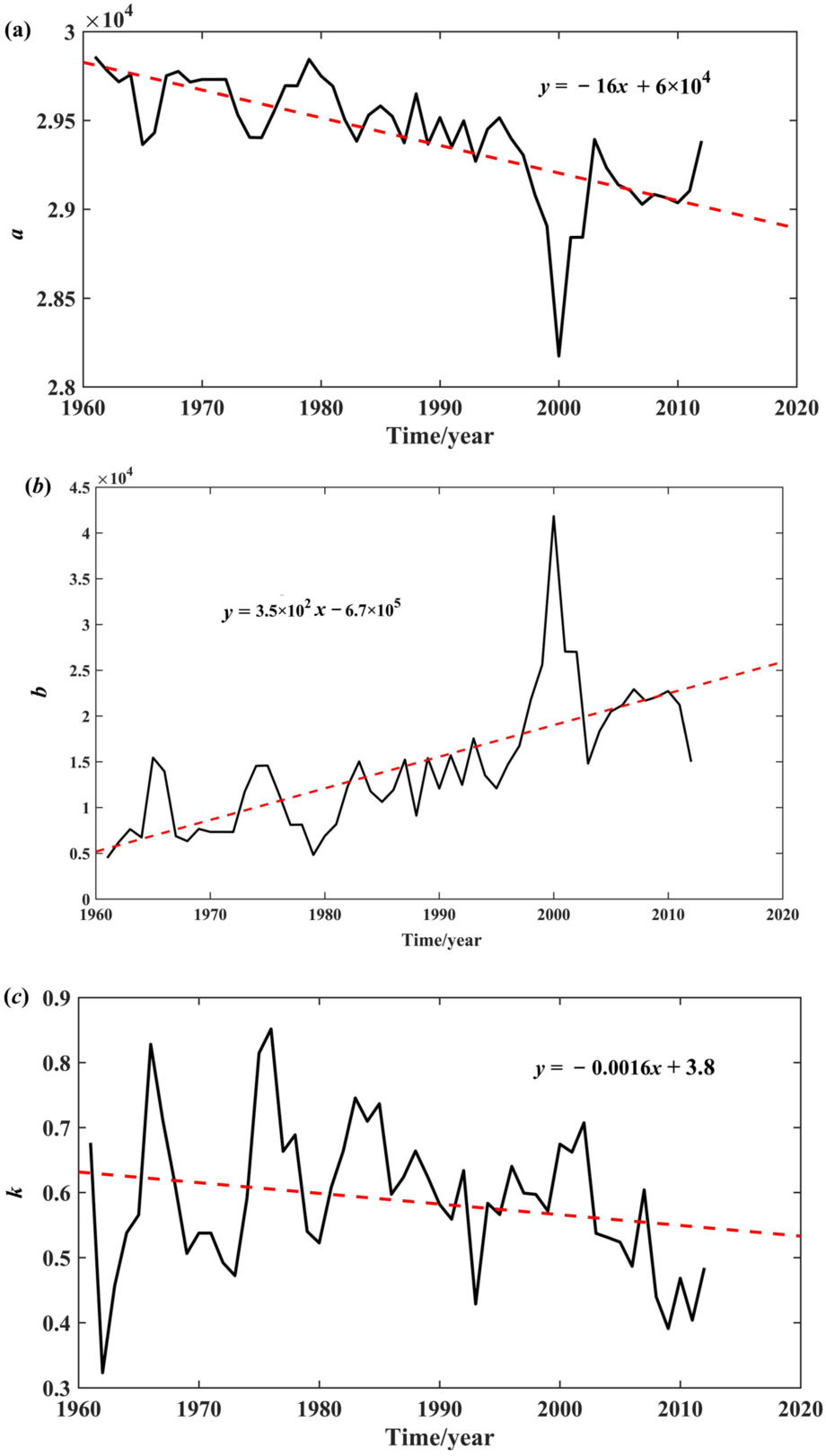

Figure 9. Temporal variation of parameters of (**a**) Parameter *a*, (**b**) Parameter *b* and (**c**) Parameter *k* at the Wangdaohengta station. The solid lines represent the value of parameters and dotted lines represent the linear fitting.

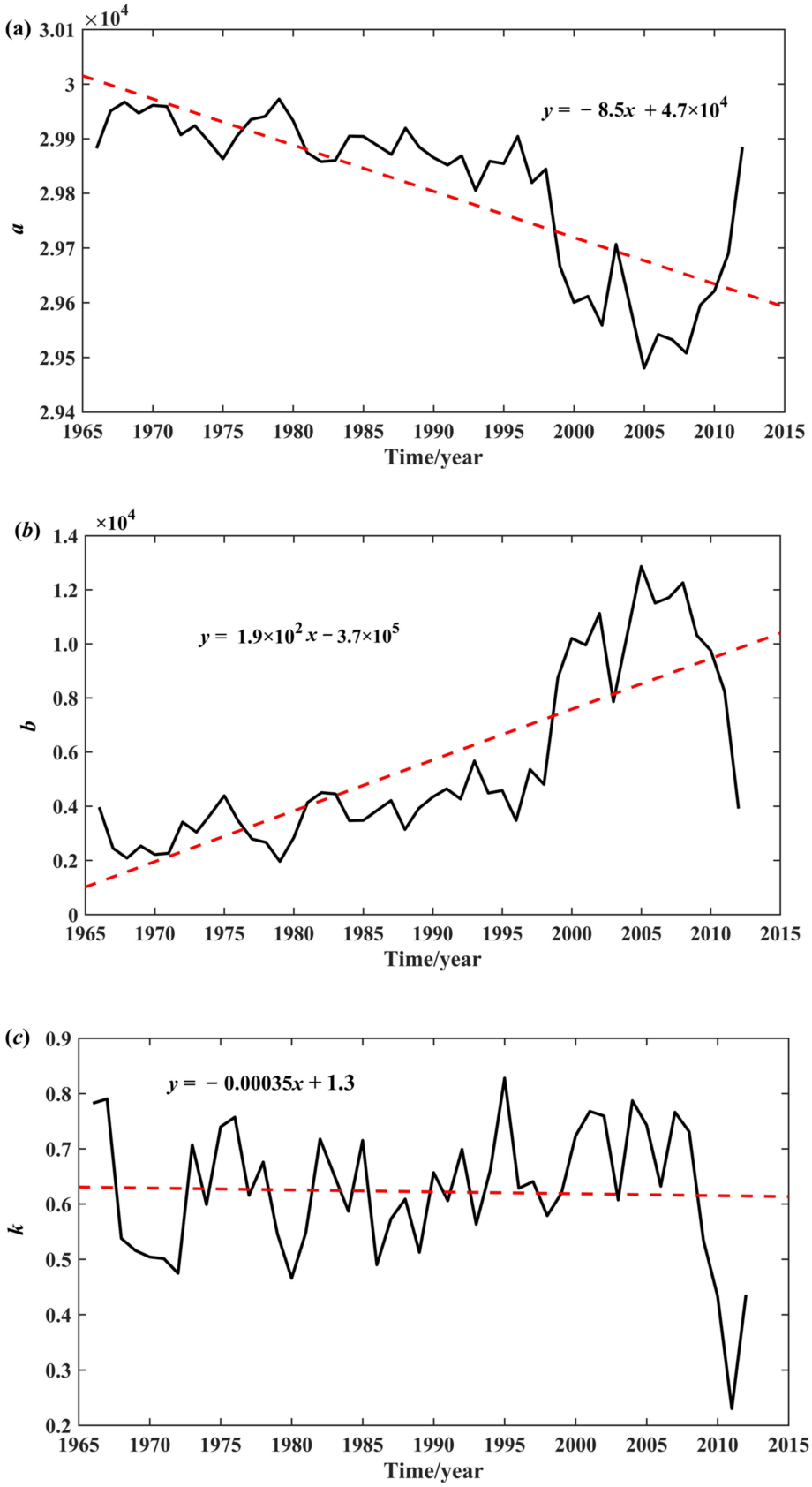

Figure 10. Temporal variation of parameters of (**a**) Parameter *a*, (**b**) Parameter *b* and (**c**) Parameter *k* at the Wenjiachuan station. The solid lines represent the value of parameters and dotted lines represent the linear fitting.

6. Conclusions

With the impact of human activity and climate change, runoff is continually changing, and the majority of the region's minor watersheds are unmeasured, with insufficient flow data. Therefore, it is essential to develop formulas for FDCs that are widely applicable in the area and that may be expanded upon and used for research in a vast range of unmeasured areas. The study identifies the best function to fit the flow duration curve of a semi-arid region in North China, which is the H2018 function, and parameterizes the H2018 function of the FDCs of the region in order to estimate the FDCs of ungauged basins.

The generalized Pareto, H2018, and log-normal distribution functions are used to fit the flow duration curves of daily discharge at 19 stations in North China. The H2018 distribution function improves the tail and head fitting of the flow duration curve and has excellent performance to represent the flow duration curve, including zero-value discharge. The specific flows at percentiles were determined, and the ratio of the flow at different frequencies was calculated in order to better comprehend the changes of FDCs. As a result, the FDCs present an 'S-shape', in which the former and latter halves of the curve descend with large range changes, while the middle section has a smaller variation.

The parameters of a, b and k in H2018 were formulated with hydrometeorological features and basin characteristics, such as the annual runoff, precipitation, precipitation in summer, potential evapotranspiration, sub-basin area covered by hydrological stations, mean elevation, length of main channel, L, and max flow frequency x_{max}, by means of a regression model. The distributions of a, b, and k were all analyzed on both the spatial and temporal scales. Parameter a has an obvious descending trend, b has an obvious increasing trend, and k has an unobvious increasing trend. The regression formula constructed in this study can obtain a regional flow duration curve with satisfactory performance, which provides a reference for the validation of remote-sensing-based runoff data in ungauged regions.

Author Contributions: L.M.: Conceptualization, Methodology, Software, Validation, Visualization, Writing—original draft, Writing—review and editing. D.L.: Methodology, Software, Research Methods Provided, Writing—original draft, Supervision, Writing—review and editing, Funding acquisition, Resources. Q.H.: Supervision, review and modification. F.G.: Analysis of data, Writing—review and editing. X.Z.: Method instruction, Writing—review and editing. J.Z.: Method instruction, Writing—review and editing. J.L.: Writing—review and editing, Resources. J.F.: Writing–review and editing, Funding acquisition. G.M.: Writing—review and editing, Funding acquisition. All authors have read and agreed to the published version of the manuscript.

Funding: This research was supported by the National Natural Science Foundation of China (NSFC) (Grant Nos. 42071335, 52279025, 52109031 and 52009102), and State Key Laboratory of Eco-hydraulics in Northwest Arid Region, China (Grant No. 2019KFKT-4).

Institutional Review Board Statement: Not applicable.

Informed Consent Statement: Not applicable.

Data Availability Statement: The DEM data used in this study were from the official website of the US Geological Survey, and which were extracted from the NASA Advanced Spaceborne Thermal Emission and Reflection Radiometer Global Digital Elevation Model (ASTER GDEM). The precipitation data can be obtained from the China Mete-orological Data Sharing Service Network (http://data.cma.cn, accessed on 14 December 2022). The other data can be obtained from the corresponding author (Dengfeng Liu, liudf@xaut.edu.cn) upon reasonable request.

Conflicts of Interest: The authors declare no conflict of interest.

References

1. Hrachowitz, M.; Savenije, H.H.G.; Blöschl, G.; McDonnell, J.J.; Sivapalan, M.; Pomeroy, J.W.; Arheimer, B.; Blume, T.; Clark, M.P.; Ehret, U.; et al. A decade of Predictions in Ungauged Basins (PUB)—A review. *Hydrol. Sci. J.* **2013**, *58*, 1198–1255. [CrossRef]
2. Young, A.R. Stream flow simulation within UK ungauged catchments using a daily rainfall-runoff model. *J. Hydrol.* **2006**, *320*, 155–172. [CrossRef]

3. Teutschbein, C.; Grabs, T.; Laudon, H.; Karlsen, R.H.; Bishop, K. Simulating streamflow in ungauged basins under a changing climate: The importance of landscape characteristics. *J. Hydrol.* **2018**, *561*, 160–178. [CrossRef]
4. Wolff, W.; Duarte, S.N. Toward geostatistical unbiased predictions of flow duration curves at ungauged basins. *Adv. Water Resour.* **2021**, *152*, 103915. [CrossRef]
5. Grimaldi, S.; Volpi, E.; Langousis, A.; Papalexiou, S.M.; De Luca, D.L.; Piscopia, R.; Nerantzaki, S.D.; Papacharalampous, G.; Petroselli, A. Continuous hydrologic modelling for small and ungauged basins: A comparison of eight rainfall models for sub-daily runoff simulations. *J. Hydrol.* **2022**, *610*, 127866. [CrossRef]
6. Yu, P.S.; Yang, T.C. Using synthetic flow duration curves for rainfall-runoff model calibration at ungauged sites. *Hydrol. Process* **2000**, *14*, 117–133. [CrossRef]
7. Worland, S.C.; Steinschneider, S.; Asquith, W.; Knight, R.; Wieczorek, M. Prediction and inference of flow duration curves using multioutput neural networks. *Water Resour. Res.* **2019**, *55*, 6850–6868. [CrossRef]
8. Kim, D.; Kaluarachchi, J. Predicting streamflows in snowmelt-driven watersheds using the flow duration curve method. *Hydrol. Earth Syst. Sci.* **2014**, *18*, 1679–1693. [CrossRef]
9. Mimikou, M.; Kaemaki, S. Regionalization of flow duration characteristics. *J. Hydrol.* **1985**, *82*, 77–91. [CrossRef]
10. Shao, Q.; Zhang, L.; Chen, Y.D.; Singh, V.P. A new method for modelling flow duration curves and predicting streamflow regimes under altered land-use conditions/une nouvelle méthode de modélisation des courbes de débits classés et de prévision des régimes d'écoulement sous conditions modifiées d'occupation du sol. *Hydrol. Sci. J.* **2009**, *54*, 606–622. [CrossRef]
11. Booker, D.J.; Snelder, T.H. Comparing methods for estimating flow duration curves at ungauged sites. *J. Hydrol.* **2012**, *434–435*, 78–94. [CrossRef]
12. Majone, B.; Avesani, D.; Zulian, P.; Fiori, A.; Bellin, A. Analysis of high streamflow extremes in climate change studies: How do we calibrate hydrological models? *Hydrol. Earth Syst. Sci. Discuss.* **2021**, *26*, 3863–3883. [CrossRef]
13. Ridolfi, E.; Kumar, H.; Bárdossy, A. A methodology to estimate flow duration curves at partially ungauged basins. *Hydrol. Earth Syst. Sci.* **2020**, *24*, 2043–2060. [CrossRef]
14. Fennessey, N.; Vogel, R.M. Regional Flow-Duration Curvesfor Ungauged Sites in Massachusetts. *J. Water Resour. Plan. Manag.* **1990**, *116*, 530–549. [CrossRef]
15. Rianna, M.; Efstratiadis, A.; Russo, F.; Napolitano, F.; Kout-soyiannis, D. A stochastic index method for calculating annual flow duration curves in intermittent rivers. *Irrig. Draunage* **2013**, *62*, 41–49. [CrossRef]
16. Rianna, M.; Russo, F.; Napolitano, F. Stochastic indexmodel for intermittent regimes: From preliminary analysis toregionalisation. *Nat. Hazards Earth Syst. Sci.* **2011**, *11*, 1189–1203. [CrossRef]
17. Pugliese, A.; Farmer, W.H.; Castellarin, A.; Archfield, S.A.; Vogel, R.M. Regional flow duration curves: Geostatistical techniques versus multivariate regression. *Adv. Water Resour.* **2016**, *96*, 11–22. [CrossRef]
18. Ganora, D.; Claps, P.; Laio, F.; Viglione, A. An approach to estimate nonparametric flow duration curves in ungauged basins. *Water Resour. Res.* **2009**, *45*, W10418. [CrossRef]
19. Archfield, S.A.; Vogel, R.M. Map correlation method: Selection of a reference streamgage to estimate daily streamflow at ungaged catchments. *Water Resour. Res.* **2010**, *46*, W10513. [CrossRef]
20. Mohamoud, Y.M. Prediction of daily flow duration curves and streamflow for ungauged catchments using regional flow duration curves. *Hydrol. Sci. J.* **2008**, *53*, 706–724. [CrossRef]
21. Farmer, W.H.; Archfield, S.A.; Over, T.M.; Hay, L.E.; LaFontaine, J.H.; Kiang, J.E. *A Comparison of Methods to Predict Historical Daily Streamflow Time Series in the Southeastern United States*; US Geological Survey: Reston, VA, USA, 2014; 34p. [CrossRef]
22. Worland, S.C.; Steinschneider, S.; Farmer, W.; Asquith, W.; Knight, R. Copula Theory as a Generalized Framework for Flow-Duration Curve Based Streamflow Estimates in Ungaged and Partially Gaged Catchments. *Water Resour. Res.* **2019**, *55*, 9378–9397. [CrossRef]
23. Hughes, D.A.; Smakhtin, V. Daily flow time series patching or extension: A spatial interpolation approach based on flow duration curves. *Hydrol. Sci. J.* **1996**, *41*, 851–871. [CrossRef]
24. Fu, B.; Wang, S.; Liu Yu Liu, J.; Liang, W.; Miao, C. Hydrogeomorphic ecosystem responses to natural and anthropogenic changes in the Loess Plateau of China. *Annu. Rev. Earth Planet. Sci.* **2017**, *45*, 223–243. [CrossRef]
25. Wang, Z.; Xu, M.; Liu, X.; Singh, D.K.; Fu, X. Quantifying the impact of climate change and anthropogenic activities on runoff and sediment load reduction in a typical Loess Plateau watershed. *J. Hydrol. Reg. Stud.* **2022**, *39*, 2214–5818. [CrossRef]
26. The Ministry of Water Resources; the National Development and Reform Commission. *Implemented the "14th Five-Year Plan" for the Construction of Silt Dams in the Yellow River Basin and the Comprehensive Control of Soil Erosion on Sloping Farmland*; Ministry of Water Resources of the People's Republic of China: Beijing, China, 2021.
27. Blum Annalise, G.; Archfield Stacey, A.; Vogel Richard, M. On the probability distribution of daily streamflow in the United States. *Hydrol. Earth Syst. Sci.* **2017**, *21*, 3093–3103. [CrossRef]
28. Westerberg, I.K.; Guerrero, J.L.; Younger, P.M.; Beven, K.J.; Seibert, J.; Halldin, S.; Freer, J.E.; Xu, C.-Y. Calibration of hydrological models using flow-duration curves. *Hydrol. Earth Syst. Sci.* **2011**, *15*, 2205–2227. [CrossRef]
29. Han, S.; Tian, F. Derivation of a sigmoid generalized complementary function for evaporation with physical constraints. *Water Resour. Res.* **2018**, *54*, 1734–1736. [CrossRef]
30. Zhao, G.; Mi, X.; Wen, Z.; Wang, F.; Gao, P. Soil erosion, conservation, and eco-environment changes in the loess plateau of china. *Land Degrad. Dev.* **2013**, *24*, 499–510. [CrossRef]

31. Song, J.; Yang, Z.; Xia, J.; Cheng, D. The impact of mining-related human activities on runoff in northern Shaanxi, China. *J. Hydrol.* **2021**, *126235*, 598. [CrossRef]
32. Li, C.; Wu, P.T.; Li, X.L.; Zhou, T.W.; Sun, S.K.; Wang, Y.B.; Luan, X.B.; Yu, X. Spatial and temporal evolution of climatic factors and its impacts on potential evapotranspiration in Loess Plateau of Northern Shaanxi, China. *Sci. Total Environ.* **2017**, *589*, 165–172. [CrossRef]
33. Luan, J.; Liu, D.; Lin, M.; Huang, Q. The construction of the flow duration curve and the regionalization parameters analysis in the northwest of china. *J. Water Clim. Change* **2021**, *12*, 2639–2653. [CrossRef]
34. Nash, I.E.; Sutcliffe, I.V. River flow forecasting through conceptual models part i—A discussion of principles-sciencedirect. *J. Hydrol.* **1970**, *10*, 282–290. [CrossRef]
35. Lane, P.N.J.; Best, A.E.; Hickel, K.; Zhang, L. The response of flow duration curves to afforestation. *J. Hydrol.* **2005**, *310*, 253–265. [CrossRef]
36. Nruthya, K.; Srinivas, V.V. Evaluating methods to predict streamflow at ungauged sites using regional flow duration curves: A case study. *Aquat. Procedia* **2015**, *4*, 641–648. [CrossRef]
37. Nagelkerke, N.J.D. A note on a general definition of the coefficient of determination. *Biometrika* **1991**, *78*, 691–692. [CrossRef]
38. Madsen, H. Automatic calibration of a conceptual rainfall–runoff model using multiple objectives. *J. Hydrol.* **2000**, *235*, 276–288. [CrossRef]
39. Shafii, M.; De Smedt, F. Multi-objective calibration of a distributed hydrological model (WetSpa) using a genetic algorithm. *Hydrol. Earth Syst. Sci.* **2009**, *13*, 2137–2149. [CrossRef]
40. Viola, F.; Noto, L.V.; Cannarozzo, M.; La Loggia, G. Regional flow duration curves for ungauged sites in sicily. *Hydrol. Earth Syst. Sci.* **2011**, *15*, 323–331. [CrossRef]
41. Abebe, S.A.; Qin, T.; Zhang, X.; Yan, D. Wavelet transform-based trend analysis of streamflow and precipitation in Upper Blue Nile River basin. *J. Hydrol. Reg. Stud.* **2022**, *44*, 2214–5818. [CrossRef]
42. Güçlü, Y.S. Improved visualization for trend analysis by comparing with classical Mann-Kendall test and ITA. *J. Hydrol.* **2020**, *584*, 124674. [CrossRef]
43. Panthi, J.; Talchabhadel, R.; Ghimire, G.R.; Sharma, S.; Dahal, P.; Baniya, R.; Boving, T.; Pradhanang, S.M.; Parajuli, B. Hydrologic regionalization under data scarcity: Implications for streamflow prediction. *J. Hydrol. Eng.* **2021**, *26*, 05021022. [CrossRef]
44. Fouad, G.; Loáiciga, H.A. Independent variable selection for regression modeling of the flow duration curve for ungauged basins in the united states. *J. Hydrol.* **2020**, *587*, 124975. [CrossRef]
45. Garbe, J.; Beevers, L.; Pender, G. The interaction of low flow conditions and spawning brown trout (Salmo trutta) habitat aviability. *Ecol. Eng.* **2016**, *88*, 53–63. [CrossRef]
46. Hasan, H.H.; Razali, S.F.M.; Muhammad, N.S.; Hamzah, F.M. Assessment of probability distributions and analysis of the minimum storage draft rate in the equatorial region. *Nat. Hazards Earth Syst. Sci.* **2021**, *21*, 1–19. [CrossRef]
47. Tomaszewski, E.; Kubiak-Wójcicka, K. Low-flows in Polish Rivers. In *Management of Water Resources in Poland*; Springer: Cham, Switzerland, 2021; pp. 205–228. [CrossRef]
48. Luan, J.; Zhang, Y.; Tian, J.; Meresa, H.; Liu, D. Coal mining impacts on catchment runoff. *J. Hydrol.* **2020**, *589*, 125101. [CrossRef]
49. Tian, L.; Jin, J.; Wu, P.; Niu, G.Y. Quantifying the impact of climate change and human activities on streamflow in a semi-arid watershed with the budyko equation incorporating dynamic vegetation information. *Water* **2018**, *10*, 1781. [CrossRef]
50. Liang, W.; Bai, D.; Jin, Z.; You, Y.; Li, J.; Yang, Y. A study on the streamflow change and its relationship with climate change and ecological restoration measures in a sediment concentrated region in the loess plateau, China. *Water Resour. Manag.* **2015**, *29*, 4045–4060. [CrossRef]
51. Xiang, Z.; Ds, A.; Mh, C.; Gw, D.; Yi, L.A. Understanding the influencing factors (precipitation variation, land use changes and check dams) and mechanisms controlling changes in the sediment load of a typical loess watershed, China. *Ecol. Eng.* **2021**, *163*, 106198. [CrossRef]